Chapter 6
Robust Displacement and Mixed CUF-Based Four-Node and Eight-Node Quadrilateral Plate Elements

Thi Huyen Cham Le, Michele D'Ottavio, Philippe Vidal, and Olivier Polit

Abstract This paper presents two classes of new four-node and eight-node quadrilateral finite elements for composite plates. Variable kinematics plate models are formulated in the framework of Carrera's Unified Formulation, which encompass Equivalent Single Layer as well as Layer-Wise models, with the variables that are defined by polynomials up to 4th order along the thickness direction z. The two classes refer to two variational formulations that are employed to derive the finite elements matrices, namely the Principle of Virtual Displacement (PVD) and Reissner's Mixed Variational Theorem (RMVT). For the PVD based elements, the main novelty consists in the extension of two field compatible approximations for the transverse shear strain field, referred to as QC4 and CL8 interpolations, which eliminate the shear locking pathology by constraining only the $z-$constant transverse shear strain terms, to all variable kinematics plate elements. Moreover, for the first time the QC4 and CL8 interpolations are introduced for the transverse shear stress field within RMVT based elements. Preliminary numerical studies are proposed on homogeneous isotropic plates that demonstrate the absence of spurious modes and of locking problems as well as the enhanced robustness with respect to distorted element shapes. The new QC4 and CL8 variable kinematics plate elements display excellent convergence rates and yield accurate responses for both, thick and thin plates.

6.1 Introduction

Composite laminates and sandwich structures are increasingly used in engineering application because of their excellent mechanical properties such as high specific stiffness and strength. Due to geometric considerations, these structures are often

Thi Huyen Cham Le · Michele D'Ottavio · Philippe Vidal · Olivier Polit
UPL, Univ Paris Nanterre, LEME, 50 Rue de Sèvres, 92410 Ville d'Avray, France
e-mail: thihuyencham.le@parisnanterre.fr,mdottavi@parisnanterre.fr
e-mail: pvidal@parisnanterre.fr,opolit@parisnanterre.fr

H. Altenbach et al. (eds.), *Analysis and Modelling of Advanced Structures and Smart Systems*, Advanced Structured Materials 81,
https://doi.org/10.1007/978-981-10-6895-9_6

described by two-dimensional plate or shell models for the design and simulation aspects. It is necessary to develop the computational models for accurate knowledge of both global and local response. However, the classical approaches, i.e., the Classical Laminate Plate Theory (CLPT) and the First-order Shear Deformation Theory (FSDT) (Reddy, 2004), are not sufficient for a predictive and accurate modeling due to complicating effects, such as anisotropy, heterogeneity and transverse shear compliance. Based on Kirchhoff-Love assumptions, CLPT neglects transverse shear deformation in the laminates. FSDT is based on Reissner-Mindlin plate theory and the transverse shear strain is assumed to be constant over the entire plate thickness. A shear correction factor is thus required to tune the accuracy of transverse shear deformation of the model.

Various two-dimensional plate theories categorize into two groups as (*i*) Equivalent Single Layer (ESL) and (*ii*) Layer-Wise (LW) models (Reddy, 1993). In the ESL approach, the number of unknowns is independent of the number of layers constituting the plate. CLPT, FSDT and the high-order shear deformation theories (HSDT) are mostly used for ESL models. HSDT are constructed by enhancing the kinematics for the transverse shear deformation and retaining the plane stress condition. No shear correction factors are required in HSDT. Several representative HSDT have been developed, e.g., Reddy's third-order theory (Reddy, 1984) and the Sinus model of Touratier (1991). An overview of ESL models can be found in Sayyad and Ghugal. (2015).

By employing a single approximation for the displacement field across all layers of the laminate, the continuity of the transverse shear and normal stress at the interface between adjacent layers with different material properties cannot be fulfilled. Zig-Zag theories describe a piece-wise continuous displacement field in the thickness direction and are, hence, able to satisfy the interlaminar continuity condition for the transverse stresses (Demasi, 2012). Note that several Zig-Zag theories have been proposed, which do not exactly fulfill the interlaminar continuity of transverse stresses, see, e.g., Barut et al (2013). The paper by Carrera (2003a) reviews several independent ways of introducing Zig-Zag theories proposed for the analysis of multilayered plates and shells. An interesting approach relies on the use of Reissner's Mixed Variational Theorem (RMVT) (Reissner, 1984), which allows to introduce independent approximations for the displacement and transverse stress fields (Carrera, 2001). Tessler (2015) proposed a Zig-Zag theory by employing RMVT in a two-step procedure. In the context of RMVT, the so-called Murakami's Zig-Zag function (MZZF) provides a simple means for representing displacement fields with a slope discontinuity at the layers' interfaces (Murakami, 1986). More recently, MZZF has been used to enhance displacement-based ESL models (Carrera, 2004; Vidal and Polit, 2011).

More accurate predictions of short wavelength responses, however, require an explicit representation of individual layers, which calls for a LW approach, see, e.g., the seminal paper by Sun and Whitney (1973) and the comprehensive discussion by Robbins Jr and Reddy (1993). Several works develop the LW models within a displacement-based approach (Reddy, 1987; Ferreira, 2005) and within the mixed

RMVT formulation (Toledano and Murakami, 1987; Carrera, 1998, 2000; Rao and Desai, 2004).

The resulting computational model of a LW approach has a number of unknowns that depends on the number of constituting layers, which can become very large. Several approaches have been thus proposed in order to reduce the computational cost by limiting the use of the expensive high-order models to small regions hosting the local stress gradient of interest, while lower-order models are used for large portions of the structure characterized by smooth, long wavelength gradients. In the framework of the finite element method we can mention the direct interface coupling (Robbins Jr and Reddy, 1996; Carrera et al, 2013), which can be enhanced on the basis of an extended variational formulation (Wenzel et al, 2014), the transition element approach (Feng and Hoa, 1998; Carrera et al, 2017), and the overlapping mesh approach based on Arlequin method (Hu et al, 2009).

A flexible manner for introducing a general description of two-dimensional formulations for modeling the composite structures has been proposed by Carrera thanks to a dedicated Unified Formulation (Carrera, 2003b). By an extensive use of compact index notations, Carrera's Unified Formulation (CUF) permits to implement a series of hierarchical, variable kinematics models within a single program by using a limited number of model-invariant 3×3 *fundamental nuclei*. In CUF, the model is constructed by using the order N for the polynomial expansion for all unknown functions; different models can be then obtained upon penalizing some specific terms (Carrera et al, 2014, 2015). Further generalizations of CUF have been proposed in Demasi (2008, 2010, 2013); Botshekanan Dehkordi et al (2013); D'Ottavio (2016); D'Ottavio et al (2016).

The first FEM application of variable kinematics CUF models has been proposed by Carrera and Demasi (2002a,b), where the matrices of plate elements have been obtained by referring to the weak forms expressed by the Principle of Virtual Displacement (PVD) and Reissner's Mixed Variational Theorem (RMVT). The displacement field can be described in an ESL or LW manner, with the possibility of superposing MZZF to an ESL description, whereas transverse stresses are always described in an LW sense. Four-, eight- and nine-node elements have been presented with C^0 isoparametric interpolations for all unknown functions.

A robust finite element (FE) should overcome numerical pathologies, i.e., it should have only six rigid body modes without spurious zero-energy modes and it should be free from numerical lacks that could degrade the solution's accuracy in case of distorted element geometries or extreme thickness ratios.

It is well known that C^0 isoparametric displacement approximations for shear deformable plates cause a spurious over-constraint in the thin-plate limit, which dramatically underestimates the bending deformation: the transverse shear locking. Several techniques have been proposed in order to prevent this pathology affecting FSDT-based plate/shell element, most of which can be stated from hybrid-mixed approaches (Pian and Sumihara, 1995). The most commonly used techniques are reduced integration methods, which, however, entail spurious zero-energy modes (Belytschko et al, 2000), and so-called B-bar techniques (Hughes, 1987), which employ a specific constraint for transverse shear strain field. Examples of such B-bar

methods are given by the so-called Kirchhoff mode (Hughes and Tezduyar, 1981), the Assumed Natural Strain (ANS) method (MacNeal, 1982; Park et al, 1989), the Mixed Interpolation of Tensorial Components (MITC) approach (Bathe and Dvorkin, 1985), the interpolations constructed using the field-consistency paradigm (Somashekar et al, 1987), the Discrete Shear elements (Batoz and Lardeur, 1989) or the Discrete Shear Gap (DSG) elements (Bletzinger et al, 2000).

All methods mentioned above were developed for FSDT kinematics and only few works are available on variable kinematics models. A selective reduced quadrature has been used in Robbins Jr and Reddy (1993); Carrera and Demasi (2002a); D'Ottavio et al (2006). Rectangular four- and nine-node elements have been proposed upon extending the MITC approach to CUF-based displacement-based models (Carrera et al, 2010; Cinefra et al, 2013). Kulikov and Plotnikova (2016) proposed a four-node quadrilateral plate element employing a hybrid-mixed ANS approach in conjunction with a variable kinematics approach formulated in terms of Sampling Surfaces (SaS). In these works, *all* transverse shear strain terms issued from the high-order kinematics are constrained according to the adopted MITC or ANS approach. However, since high-order shear deformation terms depend on the plate thickness and will vanish in thin-plate limit, the locking behavior is produced by the first-order Reissner-Mindlin kinematics only. As a matter of fact, the convergence rates of CUF elements do not depend on the polynomial order N defining the plate kinematics (D'Ottavio et al, 2006).

Concerning RMVT-based elements, it is worth reporting the hybrid-mixed developments by Li (1989); Pian and Li (1990); Hoa and Feng (1998), whose assumed transverse stress fields lead to robust finite elements for laminated plates. More recently, nine-node plate/shell element have been proposed in which the MITC technique is employed to interpolate the transverse shear stresses (Chinosi et al, 2013; Cinefra et al, 2014).

Based on the classical CUF-based FEM of Carrera and Demasi (2002a,b), the authors have recently proposed a new robust four-node quadrilateral plate element (Le et al, 2017): a special transverse shear locking correction, denoted QC4, is formulated by referring to the field consistency paradigm and applied only to the thickness-independent part of the transverse shear strain. This method was firstly proposed by Polit *et al* for FSDT (Polit et al, 1994), and subsequently extended to a refined Sinus-based kinematics (Polit et al, 2012). The previous paper (Le et al, 2017) was limited to four-node elements and to displacement-based CUF models. The purpose of this paper is to extend the methodology for obtaining robust FE to eight-node finite elements as well as to variable kinematics CUF models based on the mixed RMVT formulation.

This paper is organized as follows: the CUF-based variable kinematics approach is recalled in Sect. 6.2 and the QC4 and CL8 FE approximations are presented for displacement- and mixed-based formulations in Sect. 6.3. The numerical results are discussed in Sect. 6.4, where a comprehensive investigation is proposed that concerns the rank of the stiffness matrix, the robustness of the element with respect to length-to-thickness ratio and mesh distortion. Finally, Sect. 6.5 summarizes the main conclusions and proposes an outlook towards further studies.

6.2 Variable Kinematics Plate Model

Let us consider a multilayered plate occupying the domain $V = \Omega \times \left\{-\frac{e}{2} \leq x_3 \leq \frac{e}{2}\right\}$ in a Cartesian coordinate system $(x,y,z) = (x_i)$, see Fig. 6.1. Unless otherwise stated, Latin indices range in $\{1,2,3\}$, Greek indices range in $\{1,2\}$ and tensorial repeated index convention is employed. Ω is the reference surface of arbitrary shape lying in the $(x_1,x_2)-$plane located for convenience at $x_3 \equiv z = 0$. The plate has constant thickness e, which is composed of $k = 1,2,\ldots N_L$ orthotropic, elastic and perfectly bonded layers, each with a thickness $e^{(k)}$ and with an orientation of the material orthotropy axes defined by the rotation angle $\theta^{(k)}$ about the thickness direction z.

6.2.1 Variational Statements

The weak forms of the governing equations suitable for obtaining the FE matrices are derived from variational statements. The plate models are constructed by referring to the displacement-based approach expressed by the PVD as well as to the mixed approach expressed by the RMVT.

6.2.1.1 The Principle of Virtual Displacements

The displacement-based approach is expressed in terms of admissible virtual displacement δu_i as

$$\iint_{\Omega} \left\{ \int_{-e/2}^{e/2} \delta\epsilon_{\alpha\beta}^{(G)} \sigma_{\alpha\beta}^{(H)} + \delta\epsilon_{i3}^{(G)} \sigma_{i3}^{(H)} \, \mathrm{d}z \right\} \mathrm{d}x \, \mathrm{d}y = \iint_{\Omega} \delta u_i \bar{t}_i \, \mathrm{d}x \, \mathrm{d}y \tag{6.1}$$

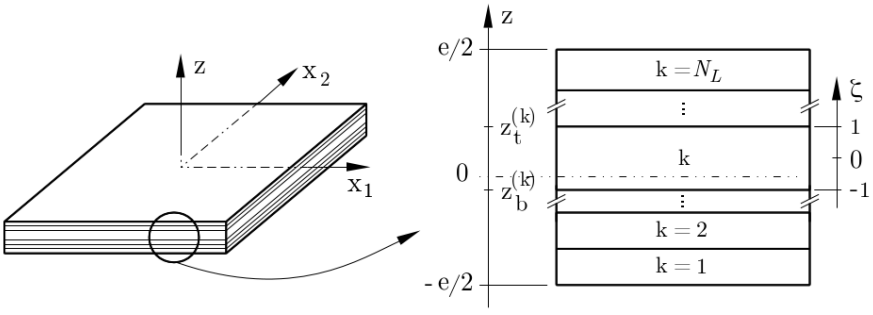

Fig. 6.1: Coordinates and notation used for the description of the composite plate.

where the imposed surface loads are denoted by $\bar{t}_i$. Eq. (6.1) yields the weak form of the equilibrium equations and traction boundary conditions once the strain field is related to the displacement by the geometric relations (superscript G)

$$\epsilon^{(G)}_{\alpha\beta} = \frac{1}{2}\left(u_{\alpha,\beta} + u_{\beta,\alpha}\right); \quad \epsilon^{(G)}_{i3} = \frac{1}{2}\left(u_{i,3} + u_{3,i}\right) \tag{6.2}$$

and the in-plane and transverse stresses are defined by means of the linear elastic constitutive law in terms of the actual strains (superscript H)

$$\begin{bmatrix} \vec{\sigma}^{(H)}_{\alpha\beta} \\ \vec{\sigma}^{(H)}_{i3} \end{bmatrix} = \begin{bmatrix} \tilde{C}_{\alpha\beta\lambda\mu} & \tilde{C}_{\alpha\beta j3} \\ \tilde{C}_{i3\lambda\mu} & \tilde{C}_{i3j3} \end{bmatrix} \begin{bmatrix} \vec{\epsilon}^{(G)}_{\lambda\mu} \\ \vec{\epsilon}^{(G)}_{j3} \end{bmatrix} \tag{6.3}$$

Exploiting the symmetry of the stress and strain tensors, Voigt compact notation is introduced for using the conventional matrix notation instead of the more cumbersome tensor notation for the description of the constitutive law Eq. (6.3). The constitutive law is obviously defined for each layer k for it depends on the layer's orthotropic elastic properties $C^{(k)}_{PQ}$ ($P, Q \in \{1,6\}$ according to Voigt notation) and on the orientation angle $\theta^{(k)}$. The generic layer k is thus assumed to have a monoclinic material symmetry in the plate's reference frame (x_α, z).

6.2.1.2 Reissner's Mixed Variational Theorem

In the framework of RMVT, the transverse stresses σ_{i3} are assumed as independent variables. The weak form of the problem can be written in terms of admissible virtual displacement δu_i and of virtual transverse stresses $\delta\sigma_{i3}$ as

$$\iint_\Omega \left\{ \int_{-e/2}^{e/2} \delta\epsilon^{(G)}_{\alpha\beta}\, \sigma^{(H)}_{\alpha\beta} + \delta\epsilon^{(G)}_{i3}\, \sigma_{i3} + \delta\sigma_{i3}\left(\epsilon^{(G)}_{i3} - \epsilon^{(H)}_{i3}\right) \mathrm{d}z \right\} \mathrm{d}x\, \mathrm{d}y = \iint_\Omega \delta u_i\, \bar{t}_i\, \mathrm{d}x\, \mathrm{d}y \tag{6.4}$$

where the transverse strains denoted by $\epsilon^{(H)}_{i3}$ and in-plane stresses $\sigma^{(H)}_{\alpha\beta}$ are evaluated by the following mixed constitutive law

$$\begin{bmatrix} \vec{\sigma}^{(H)}_{\alpha\beta} \\ \vec{\epsilon}^{(H)}_{i3} \end{bmatrix} = \begin{bmatrix} C_{\alpha\beta\lambda\mu} & C_{\alpha\beta j3} \\ C_{i3\lambda\mu} & C_{i3j3} \end{bmatrix} \begin{bmatrix} \vec{\epsilon}^{(G)}_{\lambda\mu} \\ \vec{\sigma}_{j3} \end{bmatrix} \tag{6.5}$$

where

$$\begin{cases} C_{\alpha\beta\lambda\mu} &= \tilde{C}_{\alpha\beta\lambda\mu} - \tilde{C}_{\alpha\beta i3}\, \tilde{C}^{-1}_{i3j3}\, \tilde{C}_{j3\lambda\mu} \\ C_{\alpha\beta i3} &= \tilde{C}_{\alpha\beta j3}\, \tilde{C}^{-1}_{j3i3} \\ C_{i3\alpha\beta} &= -\tilde{C}^{-1}_{i3j3}\, \tilde{C}_{j3\alpha\beta} \\ C_{i3j3} &= \tilde{C}^{-1}_{i3j3} \end{cases} \tag{6.6}$$

Voigt notation is again employed to express Eq. (6.5) and Eq. (6.6) in terms of matrices instead of fourth-order tensors. Eq. (6.4) yields the weak form of the equilibrium equations, of the traction boundary conditions and of the constitutive equations related to only the transverse stresses, i.e., the second row of Eq. (6.5). Subsidiary conditions are the geometric relations Eq. (6.2) and the constitutive equations associated to the in-plane stresses, i.e., the first row of Eq. (6.5).

6.2.2 Variable Kinematics Assumptions

According to Carrera's Unified Formulation (CUF), the two-dimensional variable kinematics plate model is formulated upon separating the in-plane variables x_α from the thickness direction z, along which a generic variable g, which may be a component of the displacement field or of the transverse stress field, i.e., $g \in \{u_i, \sigma_{i3}\}$, is *a priori* postulated by known functions $F(z)$:

$$g(x_\alpha, z) = F_\tau(z)\,\hat{g}_\tau(x_\alpha), \tag{6.7}$$

where $\tau = 0, 1, \ldots, N$ is the summation index and the order of expansion N is a free parameter of the formulation. In this work N can range from 1 to 4, in agreement with the classical CUF implementation (Carrera and Demasi, 2002a).

In order to deal with both ESL and LW descriptions within a unique notation, it is convenient to refer to a layer-specific thickness coordinate $z_k \in \{z_b^{(k)}, z_t^{(k)}\}$ that ranges between the z-coordinates of the bottom (subscript b) and top (subscript t) planes delimiting the k^{th} layer, see Fig. 6.1. Equation (6.7) can thus be formally re-written for each layer as

$$g^{(k)}(x_\alpha, z_k) = F_t(z_k)\hat{g}_t^{(k)}(x_\alpha) + F_b(z_k)\hat{g}_b^{(k)}(x_\alpha) + F_r(z_k)\hat{g}_r^{(k)}(x_\alpha) \tag{6.8}$$

with $\tau = t, b, r$ and $r = 2, \ldots N$. The variable g for the whole multilayered stack is then defined through an opportune assembly procedure of the layer-specific contributions $g^{(k)}$, which depends on the ESL or LW description.

In an ESL approach, the thickness functions are defined as Taylor-type expansion and only one variable $\hat{g}_\tau$ is used for the whole multilayer, i.e., the layer index (k) in Eq. (6.8) may be dropped off and the following thickness functions are used:

$$F_b = 1, \quad F_t = z^N, \quad F_r = z^r \quad (r = 2, \ldots N-1) \tag{6.9}$$

The ESL description can be enhanced by including the Zig-Zag function $F_{ZZ}(z)$ proposed by Murakami (1986) in order to allow slope discontinuities at layers' interfaces. In this case, the Zig-Zag function replaces the highest expansion order and the following functions are used:

$$F_b = 1, \quad F_t = F_{ZZ}(z), \quad F_r = z^r \quad (r = 2, \ldots N-1) \tag{6.10}$$

where Murakami's ZigZag Function (MZZF) is defined as

$$F_{ZZ}(z) = (-1)^k \zeta_k(z) \quad \text{with} \quad \zeta_k(z) = \frac{2}{z_t^{(k)} - z_b^{(k)}} \left(z - \frac{z_t^{(k)} + z_b^{(k)}}{2} \right) \tag{6.11}$$

Note that $F_{ZZ}(z)$ is expressed in terms of the non-dimensional layer-specific coordinate $-1 \leq \zeta_k \leq +1$ and it provides a linear piecewise function of bi-unit amplitude across the thickness of each layer k.

The assumptions for a LW description are formulated in each layer k as in Eq. (6.8), where the thickness functions are defined by linear combinations of Legendre polynomials $P_r(\zeta_k)$ as follows:

$$\begin{gathered} F_t(\zeta_k) = \frac{P_0(\zeta_k) + P_1(\zeta_k)}{2}; \quad F_b(\zeta_k) = \frac{P_0(\zeta_k) - P_1(\zeta_k)}{2}; \\ F_r(\zeta_k) = P_r(\zeta_k) - P_{r-2}(\zeta_k) \qquad (r = 2, \ldots N) \end{gathered} \tag{6.12}$$

where ζ_k is the non-dimensional coordinate introduced in Eq. (6.11). The Legendre polynomials of degree 0 and 1 are $P_0(\zeta_k) = 1$ and $P_1(\zeta_k) = \zeta_k$, respectively; higher-order polynomials are defined according to the following recursive formula:

$$P_{n+1}(\zeta_k) = \frac{(2n+1)\zeta_k P_n(\zeta_k) - n P_{n-1}(\zeta_k)}{n+1} \tag{6.13}$$

which leads to the following expressions for the polynomials employed if $N = 4$:

$$P_2(\zeta_k) = \frac{3\zeta_k^2 - 1}{2}; \quad P_3(\zeta_k) = \frac{5\zeta_k^3 - 3\zeta_k}{2}; \quad P_4(\zeta_k) = \frac{35\zeta_k^4}{8} - \frac{15\zeta_k^2}{4} + \frac{3}{8} \tag{6.14}$$

It is finally emphasized that the chosen thickness functions for a LW model satisfy the following properties

$$\begin{aligned} \zeta_k = 1: &\quad F_t = 1, \quad F_b = 0, \quad F_r = 0 \\ \zeta_k = -1: &\quad F_t = 0, \quad F_b = 1, \quad F_r = 0 \end{aligned} \tag{6.15}$$

Therefore, $\hat{g}_t^{(k)}$ and $\hat{g}_b^{(k)}$ are the physical displacement or transverse stress components at the top and bottom of the k^{th} layer, respectively, and $F_t(\zeta_k)$ and $F_b(\zeta_k)$ are the corresponding linear Lagrange interpolation functions.

6.2.3 The Stress and Strain Fields

The contributions to the strain and stress fields in each layer k are identified with respect to the in-plane (p), i.e., membrane and bending, transverse normal (n) and transverse shear (s) deformation of the plate:

$$\begin{aligned} \vec{\epsilon}_p^{(k)} &= \left[\epsilon_1^{(k)}\, \epsilon_2^{(k)}\, \epsilon_6^{(k)}\right]; \qquad \vec{\epsilon}_n^{(k)} = \epsilon_3^{(k)}; \qquad \vec{\epsilon}_s^{(k)} = \left[\epsilon_5^{(k)}\, \epsilon_4^{(k)}\right] \\ \vec{\sigma}_p^{(k)} &= \left[\sigma_1^{(k)}\, \sigma_2^{(k)}\, \sigma_6^{(k)}\right]; \qquad \vec{\sigma}_n^{(k)} = \sigma_3^{(k)}; \qquad \vec{\sigma}_s^{(k)} = \left[\sigma_5^{(k)}\, \sigma_4^{(k)}\right] \end{aligned} \tag{6.16}$$

where Voigt notation has been used.

6.2.3.1 PVD Formulation

Recalling the separation of the in-plane variables from the thickness direction, employed for expressing the assumed displacement field as in Eq. (6.8), the bending, transverse normal and transverse shear components of the strains in the displacement-based formulation are recast in the following matrix notation

$$\begin{aligned} \vec{\epsilon}_p(x_\alpha, z_k) &= Fp_{u\tau}(z_k)\, \vec{V}_\tau^{(k)}(x_\alpha) \\ \vec{\epsilon}_n(x_\alpha, z_k) &= Fn_{u\tau}(z_k)\, \vec{V}_\tau^{(k)}(x_\alpha) \\ \vec{\epsilon}_s(x_\alpha, z_k) &= Fs_{u\tau}(z_k)\, \vec{V}_\tau^{(k)}(x_\alpha) \end{aligned} \tag{6.17}$$

where $\vec{V}_\tau^{(k)}(x_\alpha)$ is the generalized strain vector of each layer defined as

$$\vec{V}_\tau^{(k)}(x_\alpha) = \left[\hat{u}_{1_\tau}^{(k)}\, \hat{u}_{1_{\tau,1}}^{(k)}\, \hat{u}_{1_{\tau,2}}^{(k)} \;\vdots\; \hat{u}_{2_\tau}^{(k)}\, \hat{u}_{2_{\tau,1}}^{(k)}\, \hat{u}_{2_{\tau,2}}^{(k)} \;\vdots\; \hat{u}_{3_\tau}^{(k)}\, \hat{u}_{3_{\tau,1}}^{(k)}\, \hat{u}_{3_{\tau,2}}^{(k)}\right]^T \tag{6.18}$$

In order to introduce the transverse shear locking correction proposed in the next section, the transverse shear strain field given in Eq. (6.17) is split into the classical $z-$constant contribution $\vec{\gamma}^0$ of standard FSDT, and a contribution $\vec{\gamma}^h$ that depends on the thickness coordinate z and is related to high-order terms:

$$\vec{\epsilon}_s(x_\alpha, z_k) = \gamma^0(x_\alpha) + \gamma^h(x_\alpha, z_k) = Fs_{u\tau}^0\, \vec{V}_\tau^{(k)}(x_\alpha) + Fs_{u\tau}^h(z_k)\, \vec{V}_\tau^{(k)}(x_\alpha) \tag{6.19}$$

Note that $Fs_{u\tau}^0$ is a matrix containing only constant values for all $z-$dependency is contained in the matrix $Fs_{u\tau}^h(z_k) = Fs_{u\tau}(z_k) - Fs_{u\tau}^0$. The explicit expressions for the matrices $Fp_{u\tau}, Fn_{u\tau}$, $Fs_{u\tau}$ and $Fs_{u\tau}^0$ can be found in Le et al (2017). The stress field is obtained by the linear elastic constitutive law Eq. (6.3).

6.2.3.2 RMVT Formulation

In addition to the compatible strains defined by Eq. (6.17), the transverse stress components are expressed in CUF as follows

$$\begin{aligned} \vec{\sigma}_n(x_\alpha, z_k) &= Fn_{\sigma\tau}(z_k)\, \vec{S}_\tau^{(k)}(x_\alpha) \\ \vec{\sigma}_s(x_\alpha, z_k) &= Fs_{\sigma\tau}(z_k)\, \vec{S}_\tau^{(k)}(x_\alpha) \end{aligned} \tag{6.20}$$

where $\vec{S}_\tau^{(k)}(x_\alpha)$ is the generalized transverse stress vector of each layer defined as

$$\vec{S}_{\tau}^{(k)}(x_{\alpha}) = \left[\hat{\sigma}_{13_{\tau}}^{(k)} \vdots \hat{\sigma}_{23_{\tau}}^{(k)} \vdots \hat{\sigma}_{33_{\tau}}^{(k)} \right]^{T} \tag{6.21}$$

and

$$Fn_{\sigma\tau} = \begin{bmatrix} 0 & 0 & F_{\tau} \end{bmatrix}, \qquad Fs_{\sigma\tau} = \begin{bmatrix} 0 & F_{\tau} & 0 \\ F_{\tau} & 0 & 0 \end{bmatrix} \tag{6.22}$$

The conjugated in-plane stresses as well as the transverse strains defined in terms of the in-plane strains and of the transverse stresses are expressed by the mixed constitutive law Eq. (6.5).

6.3 Finite Element Approximations

It is well known that the isoparametric interpolation for the transverse shear field applied to the classical displacement-based formulation leads to a locking phenomenon because of the incompatibility of the polynomial spaces defined by the sum of $\hat{u}_{\alpha_{\tau}}$ and the in-plane derivative $\hat{u}_{3_{\tau,\alpha}}$ ($\alpha = 1,2$ for γ_{13}^{0} and γ_{23}^{0}, respectively) (Polit et al, 2012). The locking pathology is associated only to the $z-$constant part, because higher-order contributions depend on the plate thickness and vanish naturally in the thin plate limit. Thus a new field-compatible interpolation for the four-node element is constructed for the $z-$constant part $\vec{\gamma}^{0}$: this is an extension to arbitrary variable kinematics plate models of the approach proposed in Polit et al (1994) for FSDT plate elements and in Polit et al (2012) to a refined plate element.

The formulation for the four-node quadrilateral FE for PVD-based CUF plate models has been reported in Le et al (2017). Therefore, this section presents at first the eight-node quadrilateral FE approximation, referred to as CL8 approximation, for avoiding transverse shear locking problems and minimizing the convergence rate loss for distorted meshes in the framework of PVD-based plate models. Subsequently, the QC4 and CL8 interpolations are employed to approximate the transverse shear stresses in the context of RMVT-based plate elements.

6.3.1 Displacement-Based Finite Elements

The CL8 interpolation is constructed as follows:

- In order to enhance the element's robustness for distorted shapes, the $z-$constant part of transverse shear strain components is written in the element's natural coordinate system $(\xi,\eta) \in [-1,+1]^2$ as:

$$\begin{bmatrix} \gamma_{\xi}^{0}(\xi,\eta) \\ \gamma_{\eta}^{0}(\xi,\eta) \end{bmatrix}^{(k)} = Fs_{u\tau}^{0} \vec{U}_{\tau}^{(k)}(\xi,\eta) \tag{6.23}$$

  where

$$\vec{U}_\tau^{(k)}(\xi,\eta) = \left[\hat{u}_{\xi_\tau}^{(k)} \hat{u}_{\xi_{\tau,\xi}}^{(k)} \hat{u}_{\xi_{\tau,\eta}}^{(k)} \vdots \hat{u}_{\eta_\tau}^{(k)} \hat{u}_{\eta_{\tau,\xi}}^{(k)} \hat{u}_{\eta_{\tau,\eta}}^{(k)} \vdots \hat{u}_{3_\tau}^{(k)} \hat{u}_{3_{\tau,\xi}}^{(k)} \hat{u}_{3_{\tau,\eta}}^{(k)} \right]^T \tag{6.24}$$

is the projection onto the reduced natural coordinates ξ,η of the generalized strain vector $\vec{V}_\tau^{(k)}$.

- The field-compatible approximation shall be constructed upon enhancing the polynomial space of the transverse deflection $\hat{u}_{3_\tau}^{(k)}$ so that its derivative matches the serendipity quadratic approximation of the in-plane displacements $\hat{u}_{\xi_\tau}^{(k)}$ and $\hat{u}_{\eta_\tau}^{(k)}$ that contribute to the $z-$constant reduced transverse shear strains γ_ξ^0 and γ_η^0. For this, a cubic polynomial interpolation is assumed for $\hat{u}_{3_\tau}^{(k)}$ by introducing four supplementary DOFs, $(\hat{u}_{3_{\tau,\xi}})_5^{(k)}$, $(\hat{u}_{3_{\tau,\eta}})_6^{(k)}$, $(\hat{u}_{3_{\tau,\xi}})_7^{(k)}$ and $(\hat{u}_{3_{\tau,\eta}})_8^{(k)}$, which correspond to the tangential derivatives of $\hat{u}_{3_\tau}$ with respect to the natural coordinates at the mid-side nodes of the reference domain, see Fig. 6.2. The supplementary DOFs are subsequently expressed in terms of the DOFs at the nodes by imposing a linear variation of the $z-$constant reduced tangential transverse shear strain at each side of the elementary domain: γ_ξ^0 should be linear along ξ at $\eta = \pm 1$ and γ_η^0 should be linear along η at $\xi = \pm 1$. The resulting eight-node FE shall be denoted CL8 due to the initial Cubic approximation for $\hat{u}_{3_\tau}$ and the subsequent Linear constraint imposed on the tangential transverse shear strains at the element's edges Polit et al (1994).
- The new field-compatible interpolation for $\gamma_\xi^0, \gamma_\eta^0$ is defined by the polynomial basis obtained from the intersection sets of monomial terms in ξ and η:

$$\begin{aligned} \mathcal{B}(\gamma_\xi^0) &= \mathcal{B}(u_{\xi_\tau}) \cap \mathcal{B}(u_{3_{\tau,\xi}}) = \left\{1, \xi, \eta, \xi\eta, \eta^2\right\} \\ \mathcal{B}(\gamma_\eta^0) &= \mathcal{B}(u_{\eta_\tau}) \cap \mathcal{B}(u_{3_{\tau,\eta}}) = \left\{1, \xi, \eta, \xi\eta, \xi^2\right\} \end{aligned} \tag{6.25}$$

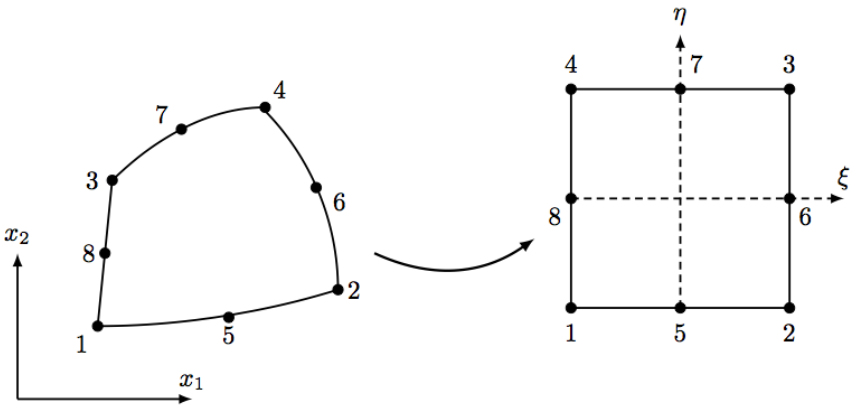

Fig. 6.2: Eight-node element in the physical Cartesian frame x_1, x_2 and in the natural frame ξ,η.

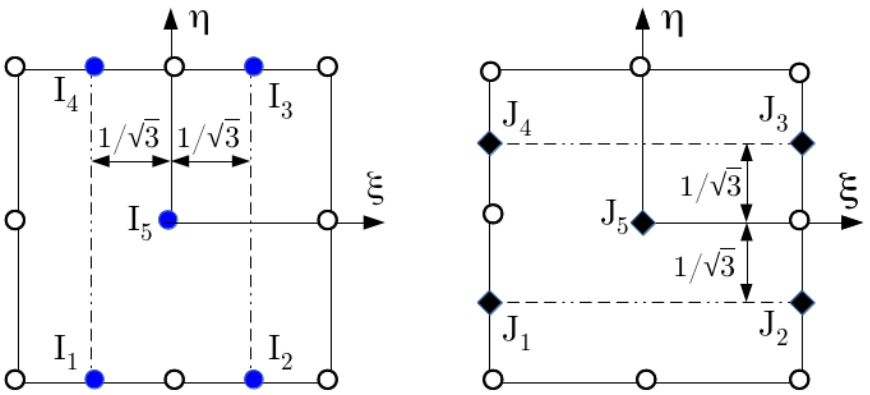

Fig. 6.3: Sampling points for CL8 finite element.

- According to the polynomial basis, five sampling points are required for each reduced transverse shear strains as illustrated in Fig. 6.3, see also Polit et al (1994). The $z-$constant reduced transverse shear strains are then obtained as follows

$$\gamma^0_\xi(\xi,\eta) = \sum_{I=1}^{5} C_{\xi I}(\xi,\eta)\,\gamma^0_{\xi I}\;; \qquad \gamma^0_\eta(\xi,\eta) = \sum_{J=1}^{5} C_{\eta J}(\xi,\eta)\,\gamma^0_{\eta J} \tag{6.26}$$

  where the interpolating functions $C_{\xi I}$ and $C_{\eta J}$ are given Appendix 1.
- The physical transverse shear strains are finally deduced from the reduced transverse shear strains in the reference domain as

$$\begin{bmatrix} \gamma^0_{13}(x_\alpha) \\ \gamma^0_{23}(x_\alpha) \end{bmatrix} = J^{-1} \begin{bmatrix} \gamma^0_\xi(\xi,\eta) \\ \gamma^0_\eta(\xi,\eta) \end{bmatrix} \tag{6.27}$$

  where

$$J = \begin{bmatrix} x_{1,\xi} & x_{2,\xi} \\ x_{1,\eta} & x_{2,\eta} \end{bmatrix} \tag{6.28}$$

  is the Jacobian matrix that will be evaluated at the 3×3 Gauss points used for integrating the stiffness matrix.

The expression for the CL8 approximation for the $z-$constant transverse shear strain field can be finally written as

$$\vec{\gamma}^0 = J^{-1}\, F s^0_{u\tau}\, \bar{B}_i\, \vec{q}^{(k)}_{\tau i} \tag{6.29}$$

where $\vec{q}^{(k)}_{\tau i} = [u^{(k)}_{1_\tau}\, u^{(k)}_{2_\tau}\, u^{(k)}_{3_\tau}]^T_i$ is the DOF vector of the node i related to the layer k and the expansion order index τ. $\bar{B}_i$ $(i = 1,8)$ is the matrix containing the modified CL8 interpolation functions and their derivatives with respect to the physical coordinates x_α. The explicit expression of the $\bar{B}_i$ matrices can be found in Appendix 2.

Starting from the integral expression Eq. (6.1), the isoparametric FE interpolations are introduced for the in-plane and transverse normal strain energy contributions, and the QC4/CL8 interpolations are introduced for the transverse shear strain energy contributions. The integral over the thickness is carried out upon assembling all layers' contributions in the appropriate manner depending on the ESL or LW description (Carrera and Demasi, 2002a,b); the integral over the in-plane domain of each finite element constituting the mesh is carried out numerically. The weak form of the equilibrium equations issued from the PVD yields thus the following standard matrix system for each finite element

$$K\,\vec{q} = \vec{f} \tag{6.30}$$

where $\vec{q}$ and $\vec{f}$ are the vectors of the nodal displacements and nodal forces. These elemental arrays are subsequently assembled over the whole mesh following the standard FEM procedure.

6.3.2 RMVT-Based Finite Elements

After introducing FE interpolations for the displacement and transverse stress fields, carrying out the integrals across the thickness (including the assembly over all layers) and the integrals over the element domain Ω_e, the RMVT integral Eq. (6.4) yields the following matrix system for each finite element

$$\begin{bmatrix} K_{uu} & K_{u\sigma} \\ {K_{u\sigma}}^T & K_{\sigma\sigma} \end{bmatrix} \begin{bmatrix} \vec{q} \\ \vec{g} \end{bmatrix} = \begin{bmatrix} \vec{f} \\ \vec{0} \end{bmatrix} \tag{6.31}$$

where $\vec{q}$ and $\vec{g}$ are the vectors of the nodal displacements and nodal transverse stresses, respectively, and $\vec{f}$ is the nodal force vector, see also Carrera and Demasi (2002a,b). The first hyper-row corresponds to the virtual variations of the displacements and represents the weak form of the equilibrium equation for the finite element, the second hyper-row corresponds to the virtual variation of the transverse stresses and represents the weak form of the transverse part of the constitutive equation of the finite element. The element contributions expressed by Eq. (6.31) can be directly assembled for the whole FE mesh, which leads to a mixed system whose unknowns are the displacements and transverse stresses at each node of the mesh.

An alternative strategy consists in statically condensing out the nodal stress unknowns of each finite element according to

$$\vec{g} = -{K_{\sigma\sigma}}^{-1}\,{K_{u\sigma}}^T\,\vec{q} \tag{6.32a}$$

which defines a mixed-hybrid formulation with only displacement DOF according to

$$\vec{K_C}\,\vec{q} = \vec{f} \qquad \text{with} \quad \vec{K_C} = \vec{K}_{uu} - \vec{K}_{u\sigma}\,{\vec{K}_{\sigma\sigma}}^{-1}\,{\vec{K}_{u\sigma}}^T \tag{6.32b}$$

The mixed-hybrid formulation Eq. (6.32) yields an element that suffers transverse shear locking if isoparametric interpolations are used for both, the displacement and the transverse stress fields (Zienkiewicz and Taylor, 2000). In order to enhance the element robustness, several strategies may be devised. One of these consists in adopting the previously discussed QC4/CL8 interpolation for the $z-$constant transverse shear strains inside the K_{uu} matrix, i.e., in correcting the compatible transverse shear strain field as in the conventional displacement-based FEM. A more interesting approach is to take profit of the mixed nature of the RMVT statement and to adopt an opportune interpolation scheme for the transverse shear stresses in conjunction with standard isoparametric interpolations for the displacement and transverse normal stress fields. It turns out that adopting the QC4 and CL8 interpolations for the transverse shear stresses yields a shear-locking-free mixed-hybrid finite element, see also Hoa and Feng (1998); Li (1989); Zienkiewicz and Taylor (2000). Therefore, the following interpolation is used in the natural reference frame for the reduced transverse shear stresses

$$\sigma_\xi(\xi,\eta) = \sum_{I=1}^{n_p} C_{\xi I}(\xi,\eta)\sigma_{\xi I}\ ; \qquad \sigma_\eta(\xi,\eta) = \sum_{J=1}^{n_p} C_{\eta J}(\xi,\eta)\sigma_{\eta J} \tag{6.33}$$

where n_p ($n_p = 2$ for QC4 and $n_p = 5$ for CL8) is the number of sampling points, which are located at the mid-sides of the edges for the four-node element (Le et al, 2017) and as illustrated in Fig. 6.3 for the eight-node element. An opportune tensorial transformation by means of the Jacobian matrix is required to map the reduced transverse shear stresses onto the physical domain.

6.4 Numerical Results

Several numerical benchmark problems are considered for displaying the accuracy and robustness of the proposed QC4 and CL8 CUF-based plate elements. The classical CUF acronyms are used for naming the various plate models: the polynomial order N is appended to a string that identifies whether the description of the displacement field is ESL (E{D,M}N), Zig-Zag (E{D,M}ZN) or LW (L{D,M}N). A capital "D" is used for PVD-based elements, while capital "M" identifies RMVT-based elements. In these latter models, the transverse stress field is always described in a LW sense. If the mixed-hybrid formulation is used for RMVT-based elements, a "c" is appended at the end of the model acronym.

Since the objective of this paper is focused on the performance of the FE approximation, the problems involve a simple homogeneous and isotropic plate. At first, the properties of the stiffness matrix are considered via an eigenvalue analysis. Subsequently, the convergence rate for thin and thick plates is investigated. Finally, the sensitivity with respect to distorted element shapes is assessed through numerical tests conducted on a square plate with distorted mesh and a circular plate. Most of the numerical tests are performed with an ESL model with expansion order $N = 2$,

which retains the three-dimensional constitutive law and avoids the occurrence of spurious Poisson locking. Table 6.1 lists the acronyms used for denoting the various configurations of boundary conditions and type of loading. Whenever possible, the computational model is reduced through application of opportune symmetry boundary conditions on the displacement field.

Present results are compared against solutions obtained with the following isoparametric approaches:

ISO full-integrated isoparametric element
ISO-SI isoparametric element with selective integration

All elements are implemented as user subroutines into the commercial ABAQUS software. A dedicated pre-processing tool allows to prepare the FE model within the ABAQUS/CAE graphical interface. Therefore, the conventional shell elements of ABAQUS will be included in the comparison, which are the general-purpose four-node elements S4 and S4R and the thick-shell eight-node element S8R. It should be noted that the S4 and S4R elements can be used for modeling thin and thick shells and both use the same transverse shear treatment, which consists in a modified version of the MITC4 assumed strain method with one Gauss point evaluation plus hourglass stabilization; the primary difference between the S4 and S4R elements is in their membrane strain field treatment (N., 2016). According to N. (2016), the use of the the S8R element should be limited to shells with non-negligible transverse shear flexibility and within a regular mesh.

6.4.1 Eigenvalues of the Stiffness Matrix

The eigenvalues of the stiffness matrix of a square element are analyzed for a thin and a thick plate, according to the following configuration

geometry square element $a \times a$ ($a = 1$), thickness $e = 10^{-n}$ ($n = 1, 3$)
material properties isotropic with $E = 10.92$ and $\nu = 0.3$

The eigenvalues of four-node displacement-based elements (ED2 model) are reported for thick and thin plates in Figs. 6.4 and 6.5, respectively. The eigenvalues of the ABAQUS general-purpose elements S4 and S4R (FSDT model) are also presented. The proposed graphics allow to recognize at a glance the eigenvalues associated to rigid-body modes as well as the gap between them and those associated to deformation modes. It is apparent that the present full integrated QC4 and ISO

Boundary conditions		Loading	
(SA)	Simply supported	(P)	Uniform load q_0 at top surface
(CL)	Clamped	(C)	Concentrated force $\bar{P}$ at plate center

Table 6.1: Acronyms for boundary conditions and type of loading.

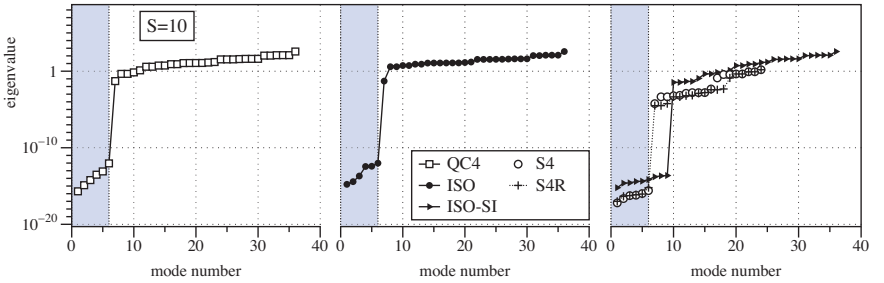

Fig. 6.4: Eigenvalues of the stiffness matrix for thick plate ($S = 10$): ED2 model, four-node FE.

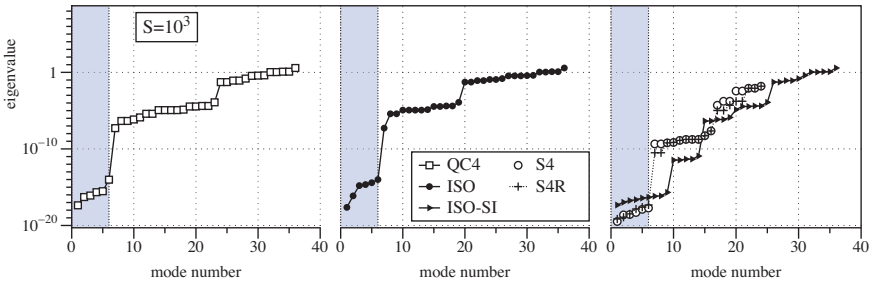

Fig. 6.5: Eigenvalues of the stiffness matrix for thin plate ($S = 1000$): ED2 model, four-node FE.

elements have the correct number of rigid-body modes (i.e., 6) regardless of the element's slenderness $S = a/e$. Similarly, the ABAQUS elements S4 and S4R do not show hourglass modes. On the contrary, the selective reduced integration scheme entails 3 spurious zero-energy modes, which indicates the possibility of an unstable behavior of both, thick and thin elements.

The same analysis is conducted on the eight-node PVD-based finite elements and the eigenvalues obtained for the thick ($S = 10$) and thin ($S = 10^3$) elements are reported in Figs. 6.6 and 6.7, respectively. As expected, the full integrated CL8 and ISO elements have six rigid-body modes independently of the plate thickness. The selective integrated eight-node element appears to have a correct rank in the thick plate case, but shows several spurious zero-energy modes in the thin plate case.The stiffness matrix of the ABAQUS S8R element shows two spurious zero-energy modes for both, the thick and the thin plate cases.

The eigenvalues of the stiffness matrix of a four-node mixed RMVT-based element are reported in Fig. 6.8 for a thick plate case and an EM2 model. The resulting FE has 36 transverse stress DOF and 36 displacement DOF, the mixed matrix has thus 72 eigenvalues. The left graphic of Fig. 6.8 reports the 36 eigenvalues that are negative and associated to the transverse stress DOF, which are thus shown to play the role

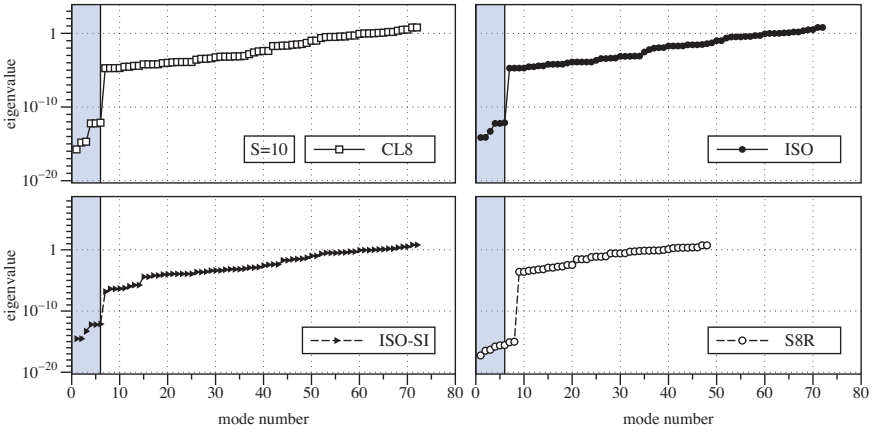

Fig. 6.6: Eigenvalues of the stiffness matrix for thick plate ($S = 10$): ED2 model, eight-node FE.

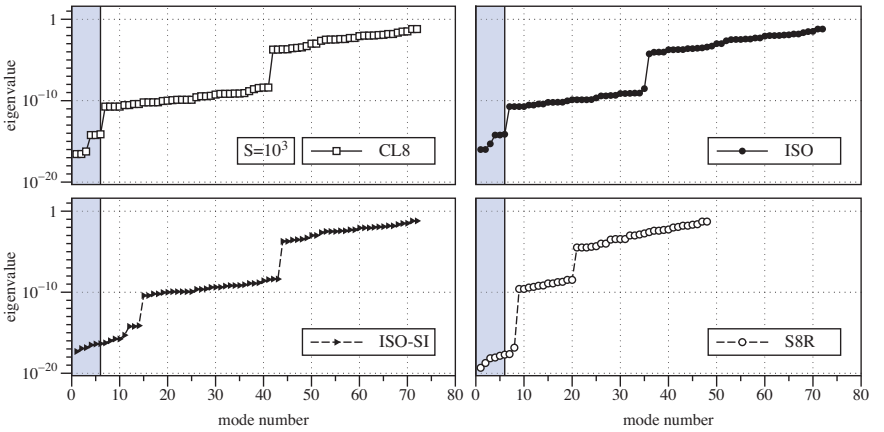

Fig. 6.7: Eigenvalues of the stiffness matrix for thin plate ($a/e = 1000$): ED2 model, eight-node FE.

of Lagrange multipliers. The graphic on the right of Fig. 6.8 displays the positive eigenvalues that are associated to the displacement DOF and shows that the proposed mixed FE with a QC4 interpolation of the transverse shear stresses has a correct rank with 6 eigenvalues that are numerically zero. It may be noted that mixed finite elements derived from Hellinger-Reissner principle possess negative eigenvalues that are related to displacement DOF, see, e.g., Mijuca (2004). Figure 6.9 reports the eigenvalues of the stiffness matrices for a mixed-hybrid 4-node element in which the transverse shear stresses are approximated either with the isoparametric or with the QC4 interpolation (the displacement field and the transverse normal stress are

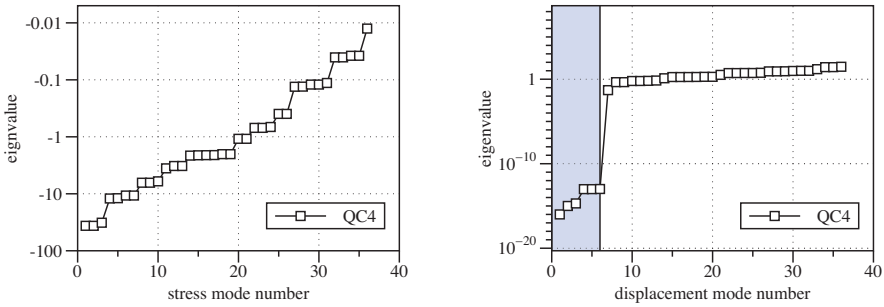

Fig. 6.8: Negative (left) and positive (right) eigenvalues of the stiffness matrix for thick plate ($S = 10$) for the full mixed EM2 model with QC4 interpolation for the transverse shear stresses.

interpolated with an isoparametric scheme). In either case, 36 positive eigenvalues are recovered, 6 of which are numerically zero. It is worth noticing that the spectra of the ISO-EM2c and of the ISO-ED2 stiffness matrices are very similar.

6.4.2 Transverse Shear Locking Test

A numerical test is carried out to assess the sensitivity of the proposed QC4 and CL8 elements to the transverse shear locking. The test is described as follows:

geometry	square plate $a \times a$ ($a = 1$), thickness $e = 10^{-n}$ with $n \in \{0,4\}$
boundary conditions	(SA) on all sides
loading	(P)
material properties	isotropic with $E = 10.92$ and $\nu = 0.3$
mesh	regular with $N = 1,2,4,8,16,32$ (see Fig. 6.10)

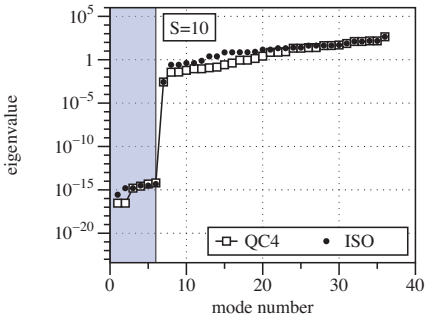

Fig. 6.9 Eigenvalues of the stiffness matrices of a mixed-hybrid 4-node EM2c element with QC4 and ISO approximations for the transverse shear stresses ($S = 10$).

results	transverse displacement U_3 at the center of the plate
reference values	Kirchhoff-Love theory (Timoshenko and Woinowsky-Krieger, 1959): $U_3^a(a/2, a/2, 0) = 0.00406\, q_0\, \frac{\mathrm{d}a^4}{\mathrm{d}t} e^3\, D$ (with $D = \frac{E}{12(1-\nu^2)}$)

The results are summarized in the two different ways.

1. Investigation of the accuracy of the FEM for a constant mesh density and varying slenderness ratio. In this case, the quarter plate is regularly meshed with $N = 4$ four-node elements or $N = 2$ eight-node elements (see Fig. 6.10). The result is the ratio between the deflection U_3 obtained by the present FEM and the reference thin plate solution U_3^a for an increasing length-to-thickness (slenderness) ratio $S = a/e$.
2. Investigation of the convergence of the FEM for a thin plate ($S = 100$). In this case, the result is reported in terms of relative error $|U_3 - U_3^a|/U_3^a$ with respect to the number N of elements used for the regular mesh of the quarter plate.

6.4.2.1 PVD Based Elements: ED2 Model

Figure 6.11 reports the ratio between the deflection U_3 obtained by the present FEM with an ED2 model and the reference thin plate solution U_3^a for an increasing length-to-thickness (slenderness) ratio $S = a/e$. Results for four-node elements and a regular mesh with $N = 4$ are given on the left, those for eight-node elements and a regular mesh with $N = 2$ are illustrated on the right.

The full integrated ISO elements are shown to suffer a very strong locking as the plate becomes thin: the linear four-node element locks severely already for $S \geq 10^2$, while the quadratic eight-node element delays the severe locking for $S \geq 10^3$. An excellent agreement with the reference Kirchhoff-Love solution is found with the new interpolation schemes QC4 and CL8, which are thus locking-free. The selective reduced quadrature scheme is shown to be effective for the linear Lagrangean four-node element, but it does not eliminate the locking pathology for the quadratic

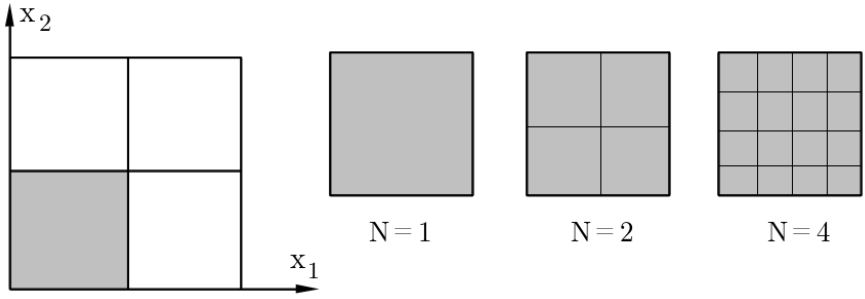

Fig. 6.10: Regular meshes for a quarter of the plate.

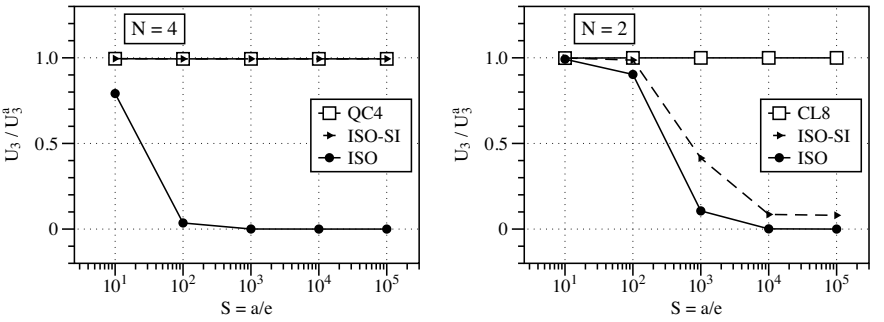

Fig. 6.11: Accuracy for a fixed mesh for thick to very thin plates: four-node (left) and eight-node (right) elements, ED2 model.

serendipity eight-node element: a severe locking is still found for ISO-SI eight-node element as $S \geq 10^3$. This difficulty is probably at the origin for the ABAQUS element S8R to be reported as suitable only for thick plates, for which the transverse shear flexibility is non-negligible.

Convergence curves for a thin plate ($S = 100$) are reported in Fig. 6.12 for the four-node elements (on the left) and the eight-node elements (on the right). Concerning the four-node FE, the locking pathology is clearly visible for the isoparametric formulation (ISO) and a good convergence rate is recovered by resorting to the selective quadrature scheme (ISO-SI) and by the present QC4 interpolation. Accurate results, with relative errors of approximately 10^{-3} in the transverse displacement, are obtained with $N = 8$ elements for the quarter plate. Concerning the eight-node FE (Fig. 6.12, right), a rather satisfying convergence rate is found for $S = 100$ and for all element formulations (ISO, ISO-SI and CL8). The new CL8 element is shown to be more accurate than the isoparametric elements, as it provides accurate results already

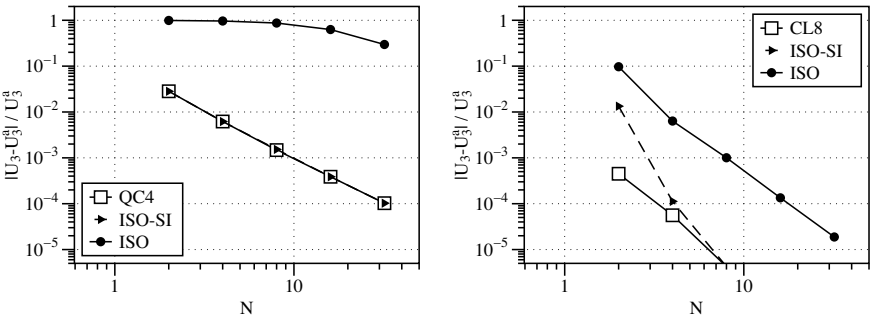

Fig. 6.12: Convergence of the transverse displacement for a thin plate ($S = 100$): four-node (left) and eight-node (right) elements, ED2 model.

with a $N = 2$ mesh for the quarter plate. As can be inferred from the right graphic of Fig. 6.11, the convergence rate of eight-node ISO and ISO-SI elements will be worse for thinner plates ($S \geq 10^3$).

6.4.2.2 RMVT Based Elements: EM2 and EM2c Models

The same analysis is carried out for RMVT based mixed-hybrid elements (EM2c model) and full mixed elements (EM2 model), where only results for the four-node elements are given for the sake of brevity. Results obtained by the mixed-hybrid approach are reported in terms of accuracy with respect to the plate slenderness and in terms of convergence towards the reference Kirchhoff-Love solution in Fig. 6.13 left and right, respectively. These results confirm that the element locks if the isoparametric interpolation is used for the displacement field and the same bi-linear interpolation is employed for the transverse shear stresses. Indeed, the EM2c ISO element behaves in exactly the same manner as the ED2 ISO element. The locking pathology can be thus corrected by resorting to a selective quadrature scheme, as first pointed out in Carrera and Demasi (2002a). More interesting, the locking pathology of the mixed-hybrid elements is eliminated by adopting the QC4 interpolation scheme for the transverse shear stresses and a full quadrature.

Results obtained by the full mixed elements EM2 are reported in Fig. 6.14. These demonstrate that the ISO element does not suffer transverse shear locking if the transverse stress DOF are not condensed out at element level. ISO elements are here shown to be merely slightly less accurate than the locking-free QC4 and ISO-SI elements.

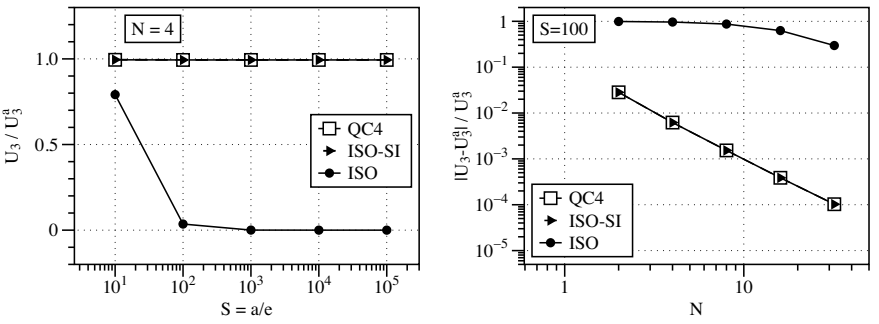

Fig. 6.13: Results of the shear locking test for the mixed-hybrid EM2c model.

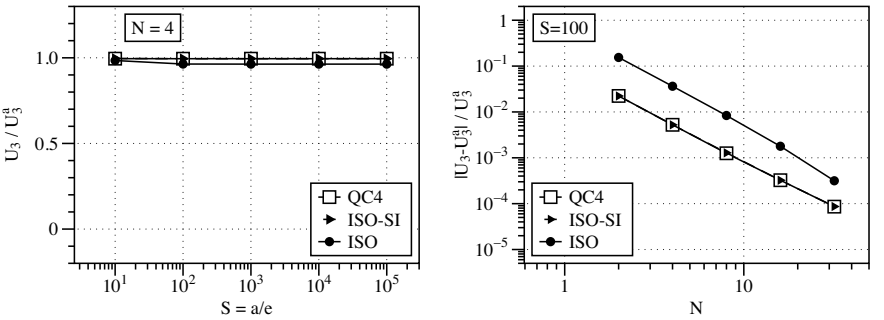

Fig. 6.14: Results of the shear locking test for the full mixed EM2 model.

6.4.2.3 Effectiveness of the QC4/CL8 Approach for Variable Kinematics Models

The shear locking test is carried out for various CUF-based elements in order to demonstrate the effectiveness of the proposed QC4 and CL8 approach irrespective of the employed plate kinematics. Only results for the four-node are shown, the very similar results obtained for the CL8 elements are omitted for the sake of brevity. Figure fig:validCUF-ShearLock illustrates the results obtained with several LW as well ESL models, formulated in the framework of PVD and RMVT, with the new QC4 finite element approximations. All curves are sensibly overlapped, which thus validates the proposed approach for all CUF-based variable kinematics models. In particular, for displacement-based elements, it is clearly sufficient to correct only the $z-$constant part of the transverse shear strain in order to eliminate the locking pathology. The independence of the FE approximation from any refinement of the FSDT kinematics has been already pointed out in D'Ottavio et al (2006).

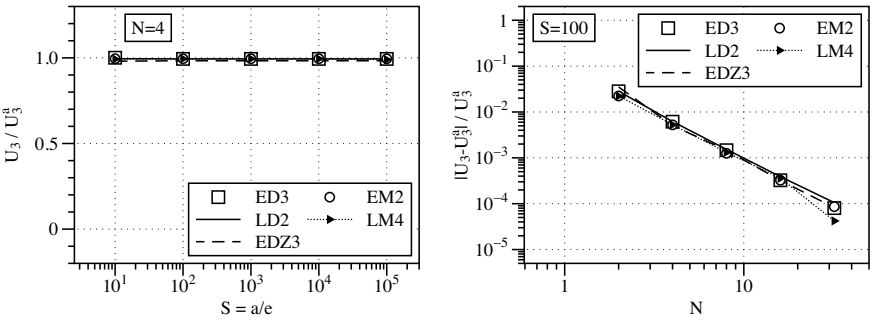

Fig. 6.15: Results of the shear locking test for various CUF models and QC4 approximation.

6.4.3 The Distortion Tests

In this section, the sensitivity of the present FE to the mesh distortion is illustrated on two test cases widely used in open literature, namely the square plate with distorted mesh and the circular plate.

6.4.3.1 The Square Plate Test

This standard test is classically used in order to investigate the mesh sensitivity in plate bending problems. The data are given as follows:

geometry	square plate $a \times a$ with $a = 100$ and thickness $e = 1$
boundary conditions	(SA) on all sides
loading	(C)
material properties	isotropic with $E = 10.92$ and $\nu = 0.3$
mesh	$N = 2$ for the quarter plate, with the distortion parameter $s \in \{-12, -8, -4, 0, 4, 8, 12\}$ – see Fig. 6.16
results	transverse displacement $U_3 = u_3(a/2, a/2, 0)$
reference value	transverse displacement $U_3^{(0)}$ for the regular mesh ($s = 0$)

The distorted meshes are characterized by the parameter s defining the coordinates of the mid-node of the quarter plate, which is located in the undistorted mesh ($s = 0$) at $X_1 = X_2 = a/4$. The parameter s may be positive or negative, as illustrated in Fig. 6.16, and it defines the coordinates of the mid-node as $(a/4 + s, a/4 + s)$: by taking $a = 100$, for the most distorted meshes ($s = \pm 12$) the mid-node is hence located at $(\pm 37, \pm 37)$. Note that it is not usual in open literature to consider positive and negative values for the parameter s. Since a concentrated load is applied at $X_1 = X_2 = a/2$, the results obtained for positive and negative values of s may not be symmetric.

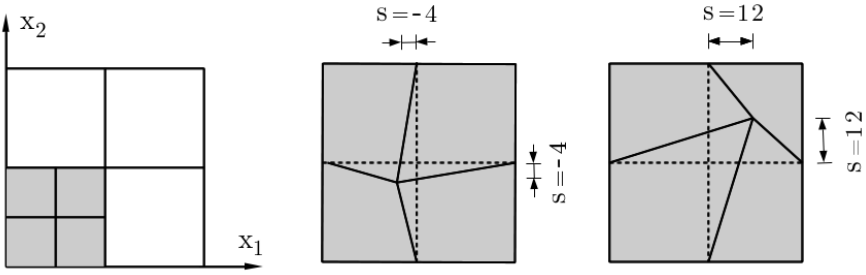

Fig. 6.16: Mesh for the quarter plate with distortion defined by the parameter s.

The transverse displacement U_3 at the center node is normalized with respect to the value U_3^0 obtained with the regular, undistorted mesh ($s = 0$). Fig. 6.17 shows the results obtained by the ED2 model: on the left are reported the curves obtained by the four-node elements while on the right those obtained by the eight-node elements. The ABAQUS finite elements S4R and S8R, are included in the comparison. The results show that the proposed QC4 and CL8 are the most robust elements with respect to mesh distortion, in particular CL8 results to be practically insensitive to the mesh distortion parameter. The highest distortion sensitivity is displayed by the full-integrated ISO elements. Selective reduced quadrature elements ISO-SI perform better than the ISO elements: in the four-node case the enhancement is seen only for $s > 0$. The ABAQUS S4R element has very similar performances of the QC4 element, whereas the S8R element closely follows the behavior of the eight-node ISO-SI element and is thus outperformed by the proposed CL8 element.

6.4.3.2 The Circular Plate Test

Another mesh distortion sensitivity test is considered, which concerns the bending of a clamped circular isotropic plate subjected to a uniform pressure load according to the following data:

geometry	circular plate of radius $R = 5$ and thickness $e = 0.1$
boundary conditions	(CL) on the external perimeter
loading	(P)
material properties	isotropic with $E = 1.7472\ 10^7$ and $\nu = 0.3$
mesh	$N = 3, 12, 28, 60$ elements for a quarter plate – see Fig. 6.18
results	deflection $U_3 = u_3(0,0,0)$ at the center of the plate

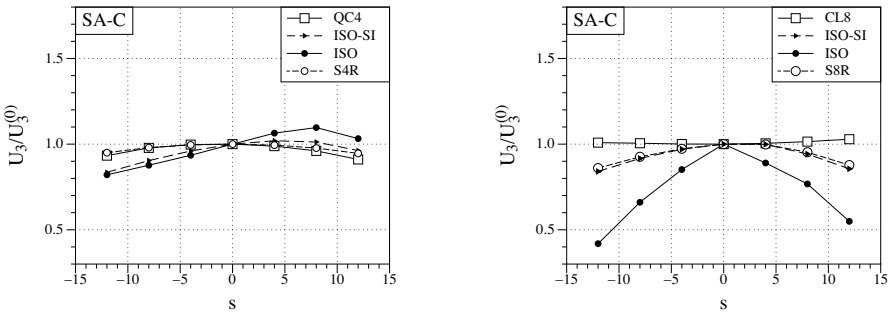

Fig. 6.17: Square plate test (SA-C): variation of the normalized central deflection with respect to the mesh distortion parameter s. Four-node (left) and eight-node elements (right), ED2 model.

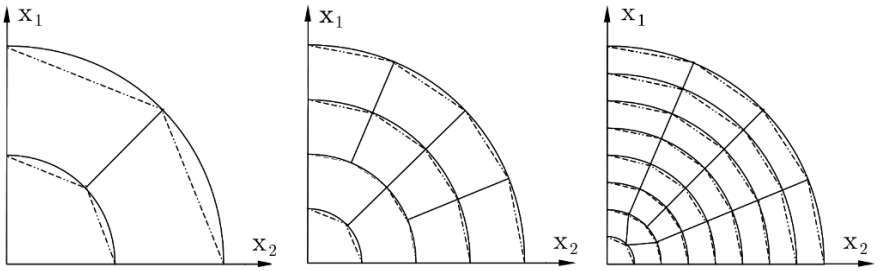

Fig. 6.18: FE meshes with $N = 3, 12, 28$ elements for a quarter of the circular plate: 8-node elements (continuous line) and 4-node elements (dotted line).

reference value	Kirchhoff-Love theory $U_3^{\text{ref}} = 0.61147\ 10^{-6}$ Batoz and Dhatt (1990)

The evolution of the ratio between the central deflection and the Kirchhoff-Love solution with respect to the mesh density is reported in Fig. 6.19. The ED2 kinematics is again used and the results obtained by ABAQUS finite elements S4R and S8R are also shown for comparison.

Concerning the four-node elements (Fig. 6.19, left), it has been already shown that the ISO element suffers the distorted shapes, and for the present case it shows errors exceeding 90% even with the more refined mesh. It can be noticed that the QC4 element has a good convergence rate and its accuracy is very satisfactory. In particular, the error becomes less than 3% for $N \geq 30$, whereas the converged result of the four-node ISO-SI FE is still affected with an error of about 10%. The ABAQUS S4R element shows a higher accuracy than the present QC4 element for coarser meshes, but the differences between S4R and QC4 are negligible as the mesh is refined.

Observing the results for the eight-node elements (Fig. 6.19, right), it is noted that the ISO element suffers the distorted shapes, but the deflection tends towards the solution as the mesh is refined ($N \geq 28$). It is further confirmed that the CL8 element is very robust, with performances that in this case are slightly better compared to those of the ABAQUS S8R element.

6.5 Conclusion

This paper has introduced robust FE interpolations for four-node and eight-node quadrilateral plate elements with variable kinematics expressed through Carrera's Unified Formulation. A previous work focused on four-node PVD-based elements Le et al (2017), has been thus extended to eight-node serendipity FE approximations as well as to RMVT-based plate models. In the framework of displacement-based models, two field-consistent transverse shear strain approximations referred to as QC4

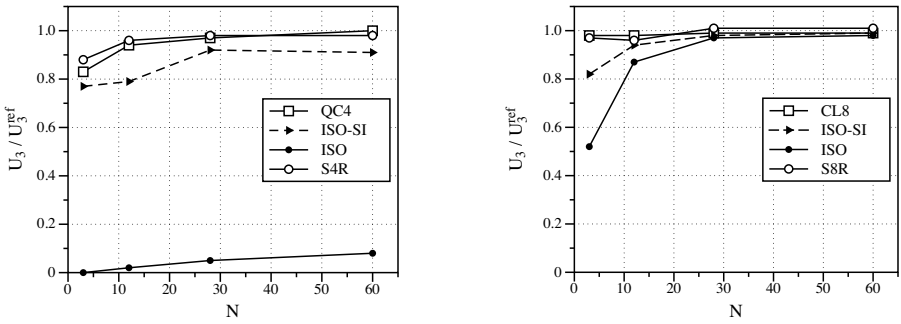

Fig. 6.19: Convergence study of the central deflection for the circular plate. Four-node (left) and eight-node elements (right), ED2 model.

and CL8 Polit et al (1994) have been extended to plate models of arbitrary kinematic order, including ESL and LW descriptions, by modifying only the $z-$constant part of the transverse shear strain. In the framework of RMVT based models, it has been shown that the full mixed formulation with isoparametric approximations does not show any shear locking pathology, but that the corresponding mixed-hybrid FEM requires an opportune correction. An enhanced mixed-hybrid FEM has been thus proposed by adopting for the transverse shear stress field the interpolation schemes resulting from the QC4 and CL8 formulations.

First results have been presented in view of assessing the robustness and accuracy of the proposed elements. For this, a number of numerical tests have been considered that are recommended whenever FE applications are proposed: eigenvalue counts to ensure the proper rank of the stiffness matrices, convergence behavior for thin and thick plates, as well as two case studies involving distorted meshes. The numerical results confirmed the superiority of the proposed FEs in comparison to classical isoparametric approaches with full or reduced integrations, i.e., they have a correct rank, are free of transverse shear locking and are less sensitive to distorted element shapes. The proposed variable kinematics FEs, implemented as a user subroutine into ABAQUS, provide a robust tool for the analysis of composite laminates, for which different models may be used for adapting the computational cost in case of thin or thick plates or whether a global or local response is required.

The preliminary results shown in this paper shall be completed by further analyses of RMVT based elements and of composite plates, including laminates and sandwich configurations. Furthermore, the optimization of the computational cost for FE models of composite structures shall be considered: on the one hand, the FE implementation of a more general variable kinematics modeling approach will be considered D'Ottavio (2016); the variable kinematics models shall, on the other hand, be effectively employed within a global-local approach that limits the use of expensive, highly accurate and quasi-3D models to small model portions.

Appendix 1

The interpolation functions on the elementary domain are defined as follows

$$
\begin{aligned}
C_{\xi 1}(\xi,\eta) &= \frac{1}{4}(-\eta-\sqrt{3}\xi)(1-\eta); \quad & C_{\eta 1}(\xi,\eta) &= \frac{1}{4}(-\xi-\sqrt{3}\eta)(1-\xi)\\
C_{\xi 2}(\xi,\eta) &= \frac{1}{4}(-\eta+\sqrt{3}\xi)(1-\eta); \quad & C_{\eta 2}(\xi,\eta) &= \frac{1}{4}(\xi-\sqrt{3}\eta)(1+\xi)\\
C_{\xi 3}(\xi,\eta) &= \frac{1}{4}(\eta+\sqrt{3}\xi)(1+\eta); \quad & C_{\eta 3}(\xi,\eta) &= \frac{1}{4}(\xi+\sqrt{3}\eta)(1+\xi)\\
C_{\xi 4}(\xi,\eta) &= \frac{1}{4}(\eta-\sqrt{3}\xi)(1+\eta); \quad & C_{\eta 4}(\xi,\eta) &= \frac{1}{4}(-\xi+\sqrt{3}\eta)(1-\xi)\\
C_{\xi 5}(\xi,\eta) &= 1-\eta^2; & C_{\eta 5}(\xi,\eta) &= 1-\xi^2
\end{aligned}
\tag{6.34}
$$

Appendix 2

The non-zero terms of the 9 x 3 matrices $\bar{B}_i$ ($i = 1,8$) defining the CL8 interpolation for $\vec{\gamma}^0$ as in Eq. (6.29) are

$$
\begin{aligned}
\bar{B}_i(1,1) &= \sum_{I=1}^{5} C_{\xi I}\left(N_i(\xi_I,\eta_I)\; J_{11}^{(I)}(\xi_I,\eta_I) + N_{i,\xi}^{RT}(\xi_I,\eta_I)\right)\\
\bar{B}_i(1,2) &= \sum_{I=1}^{5} C_{\xi I}\left(N_i(\xi_I,\eta_I)\; J_{12}^{(I)}(\xi_I,\eta_I) + N_{i,\xi}^{ST}(\xi_I,\eta_I)\right)\\
\bar{B}_i(8,3) &= \sum_{I=1}^{5} C_{\xi I}\; N_i(\xi_I,\eta_I)\\
\bar{B}_i(4,1) &= \sum_{J=1}^{5} C_{\eta J}\left(N_i(\xi_J,\eta_J)\; J_{21}^{(J)}(\xi_J,\eta_J) + N_{i,\eta}^{RT}(\xi_J,\eta_J)\right)\\
\bar{B}_i(4,2) &= \sum_{J=1}^{5} C_{\eta J}\left(N_i(\xi_J,\eta_J)\; J_{22}^{(J)}(\xi_J,\eta_J) + N_{i,\eta}^{ST}(\xi_J,\eta_J)\right)\\
\bar{B}_i(9,3) &= \sum_{J=1}^{5} C_{\eta J}\; N_i(\xi_J,\eta_J)
\end{aligned}
\tag{6.35}
$$

where $J_{\alpha\beta}^{(p)}$ ($p = 1,5$) is the Jacobian at sampling points. The isoparametric interpolation functions for node i are denoted N_i. The functions N_i^{RT} and N_i^{ST} are given as

$$
\begin{aligned}
N_{i\ (i=1,2,3,4)}^{RT}(\xi,\eta) &= \frac{1}{12}\left[-J_{11}^{N_i}\,\xi\left(\xi^2-1\right)(1+\eta_i\eta)-J_{21}^{N_i}\,(1+\xi_i\xi)\,\eta\left(\eta^2-1\right)\right]\\
N_{i\ (i=5,7)}^{RT}(\xi,\eta) &= \frac{1}{6}\left[J_{11}^{N_i}\,\xi\left(\xi^2-1\right)(1+\eta_i\eta)\right]\\
N_{i\ (i=6,8)}^{RT}(\xi,\eta) &= \frac{1}{6}\left[J_{21}^{N_i}\,(1+\xi_i\xi)\,\eta\left(\eta^2-1\right)\right]\\
N_{i\ (i=1,2,3,4)}^{ST}(\xi,\eta) &= \frac{1}{12}\left[-J_{12}^{N_i}\,\xi\left(\xi^2-1\right)(1+\eta_i\eta)-J_{22}^{N_i}\,(1+\xi_i\xi)\,\eta\left(\eta^2-1\right)\right]\\
N_{i\ (i=5,7)}^{ST}(\xi,\eta) &= \frac{1}{6}\left[J_{12}^{N_i}\,\xi\left(\xi^2-1\right)(1+\eta_i\eta)\right]\\
N_{i\ (i=6,8)}^{ST}(\xi,\eta) &= \frac{1}{6}\left[J_{22}^{N_i}\,(1+\xi_i\xi)\,\eta\left(\eta^2-1\right)\right]
\end{aligned}
\tag{6.36}
$$

where $J_{\alpha\beta}^{N_i}$ $(i=1,8)$ is the Jacobian at nodes i.

References

Barut A, Madenci E, Tessler A (2013) C^0-continuous triangular plate element for laminated composite and sandwich plates using the {2,2}-Refined Zigzag Theory. Compos Struct 106:835–853

Bathe KJ, Dvorkin EN (1985) A four-node plate bending element based on Mindlin/Reissner plate theory and a mixed interpolation. Int J Numer Meth Eng 21:367–383

Batoz JL, Dhatt G (1990) Modélisation des Structures par Eléments Finis, volume 2: Poutres et Plaques. Hermès

Batoz JL, Lardeur P (1989) A discrete shear triangular nine d.o.f. element for the analysis of thick to very thin plates. Int J Numer Meth Eng 28:533–560

Belytschko T, Liu WK, Moran B (2000) Nonlinear Finite Elements for Continua and Structures. John Wiley & Sons, LTD, 2 edition

Bletzinger KU, Bischoff M, Ramm E (2000) A unified approach for shear locking free triangular and rectangular shell finite elements. Comput Struct 75:321–334

Botshekanan Dehkordi M, Cinefra M, Khalili SMR, Carrera E (2013) Mixed LW/ESL models for the analysis of sandwich plates with composite faces. Compos Struct 98:330–339

Carrera E (1998) Evaluation of layerwise mixed theories for laminated plates analysis. AIAA J 36:830–839

Carrera E (2000) Single- vs multilayer plate modelings on the basis of Reissner's mixed theorem. AIAA J 38:342–352

Carrera E (2001) Developments, ideas and evaluations based upon Reissner's Mixed Variational Theorem in the modeling of multilayered plates and shells. Appl Mech Rev 54:301–329

Carrera E (2003a) Historical review of zig-zag theories for multilayered plates and shells. Appl Mech Rev 56:287–308

Carrera E (2003b) Theories and finite elements for multilayered plates and shells: A unified compact formulation with numerical assessment and benchmarking. Arch Comput Meth Eng 10:215–296

Carrera E (2004) On the use of Murakami's zig-zag function in the modeling of layered plates and shells. Comput Struct 82:541–554

Carrera E, Demasi L (2002a) Classical and advanced multilayered plate elements based upon PVD and RMVT. Part 1: Derivation of finite element matrices. Int J Numer Meth Eng 55(2):191–231

Carrera E, Demasi L (2002b) Classical and advanced multilayered plate elements based upon PVD and RMVT. Part 2: Numerical implementations. Int J Numer Meth Eng 55(3):253–291

Carrera E, Cinefra M, Nali P (2010) MITC technique extended to variable kinematic multilayered plate elements. Compos Struct 92:1888–1895

Carrera E, Pagani A, Petrolo M (2013) Use of Lagrange multipliers to combine 1D variable kinematic finite elements. Comput Struct 129:194–206
Carrera E, Cinefra M, Petrolo M, Zappino E (2014) Finite Element Analysis of Structures through Unified Formulation. John Wiley & Sons, Ltd
Carrera E, Cinefra M, Lamberti A, Petrolo M (2015) Results on best theories for metallic and laminated shells including layer-wise models. Compos Struct 126:285–298
Carrera E, Pagani A, Valvano S (2017) Multilayered plate elements accounting for refined theories and node-dependent kinematics. Compos B 114:189–210
Chinosi C, Cinefra M, Della Croce L, Carrera E (2013) Reissner's mixed variational theorem toward MITC finite elements for multilayered plates. Compos Struct 99:443–452
Cinefra M, Chinosi C, Della Croce L (2013) MITC9 shell elements based on refined theories for the analysis of isotropic cylindrical structures. Mech Adv Mater Struct 20:91–100
Cinefra M, Chinosi C, Della Croce L, Carrera E (2014) Refined shell finite elements based on RMVT and MITC finite elements for the analysis of laminated structures. Compos Struct 113:492–497
Demasi L (2008) ∞^3 hierarchy plate theories for thick and thin composite plates: The generalized unified formulation. Compos Struct 84:256–270
Demasi L (2010) Invariant finite element model for composite structures: The generalized unified formulation. AIAA J 48:1602–1619
Demasi L (2012) Partially Zig-Zag advanced higher order shear deformation theories based on the Generalized Unified Formulation. Compos Struct 94:363–375
Demasi L (2013) Partially Layer Wise advanced Zig Zag and HSDT models based on the Generalized Unified Formulation. Eng Struct 53:63–91
D'Ottavio M (2016) A Sublaminate Generalized Unified Formulation for the analysis of composite structures and its application to sandwich plates bending. Compos Struct 142:187–199
D'Ottavio M, Ballhause D, Wallmersperger T, Kröplin B (2006) Considerations on higher-order finite elements for multilayered plates based on a unified formulation. Comput Struct 84:1222–1235
D'Ottavio M, Dozio L, Vescovini R, Polit O (2016) Bending analysis of composite laminated and sandwich structures using sublaminate variable-kinematic Ritz models. Compos Struct 155:45–62
Feng W, Hoa SV (1998) Partial hybrid finite elements for composite laminates. Finite Elem Anal Des 30:365–382
Ferreira AJM (2005) Analysis of composite plates using a layerwise shear deformation theory and multiquadrics discretization. Mech Adv Mater Struct 12:99–112
Hoa SV, Feng W (1998) Hybrid Finite Element Method for Stress Analysis of Laminated Composites. Springer Science+Business Media, LLC, New York
Hu H, Belouettar S, Potier-Ferry M, Daya EM (2009) Multi-scale modelling of sandwich structures using the Arlequin method - Part I: Linear modelling. Finite Elem Anal Des 45:37–51
Hughes TJR (1987) The Finite Element Method. Prentice-Hall
Hughes TJR, Tezduyar T (1981) Finite elements based upon Mindlin plate theory with particular reference to the four node bilinear isoparametric element. J Appl Mech 46:587–596
Kulikov GM, Plotnikova SV (2016) A hybrid-mixed four-node quadrilateral plate element based on sampling surfaces method for 3D stress analysis. Int J Numer Meth Eng 108:26–54
Le THC, D'Ottavio M, Vidal P, Polit O (2017) A new robust quadrilateral four-node variable kinematics plate element for composite structures. Finite Elem Anal Des 113:10–24
Li MS (1989) Higher order laminated composite plate analysis by hybrid finite element method. PhD thesis, Massachusetts Institute of Technology
MacNeal RH (1982) Derivation of element stiffness matrices by assumed strain distributions. Nucl Eng Des 70:3–12
Mijuca D (2004) On hexahedral finite element HC8/27 in elasticity. Comput Mech 33:466–480
Murakami H (1986) Laminated composite plate theory with improved in-plane response. J Appl Mech 53:661–666
N N (2016) *Abaqus Theory Manual*. Dassault Systèmes

Park KC, Pramono E, Stanley GM, Cabiness HA (1989) The ANS shell elements: earlier developments and recent improvements. vol 3 of *CED*, pp 217–239

Pian THH, Li MS (1990) Stress analysis of laminated composites by hybrid finite elements. Springer-Verlag

Pian THH, Sumihara K (1995) State-of-the-art development of hybrid/mixed finite element method. Finite Elem Anal Des 21:5–20

Polit O, Touratier M, Lory P (1994) A new eight-node quadrilateral shear-bending plate finite element. Int J Numer Meth Eng 37:387–411

Polit O, Vidal P, D'Ottavio M (2012) Robust C^0 high-order plate finite element for thin to very thick structures: mechanical and thermo-mechanical analysis. Int J Numer Meth Eng 90:429–451

Rao MK, Desai YM (2004) Analytical solutions for vibrations of laminated and sandwich plates using mixed theory. Compos Struct 63:361–373

Reddy JN (1984) A simple higher-order theory for laminated composite plates. J Appl Mech 51:745–752

Reddy JN (1987) A generalization of two-dimensional theories of laminated composite plates. Comm Appl Numer Meth 3:173–180

Reddy JN (1993) An evaluation of equivalent-single-layer and layerwise theories of composite laminates. Compos Struct 25:21–35

Reddy JN (2004) Mechanics of Laminated Composite Plates and Shells: Theory and Analysis. CRC Press, 2nd edition

Reissner E (1984) On a certain mixed variational theorem and a proposed application. Int J Numer Meth Eng 20:1366–1368

Robbins Jr DH, Reddy JN (1993) Modelling of thick composites using a layerwise laminate theory. Int J Numer Meth Eng 36:655–677

Robbins Jr DH, Reddy JN (1996) Variable kinematic modeling of laminated composite plates. Int J Numer Meth Eng 39:2283–2317

Sayyad AS, Ghugal YM (2015) On the free vibration analysis of laminated composite and sandwich plates: A review of recent literature with some numerical results. Compos Struct 129:177–201

Somashekar BR, Prathap G, Babu CR (1987) A field-consistent, four-noded, laminated, anisotropic plate/shell element. Comput Struct 25:345–353

Sun CT, Whitney JM (1973) Theories for the dynamic response of laminated plates. AIAA J 11:178–183

Tessler A (2015) Refined zigzag theory for homogeneous, laminated composite, and sandwich beams derived from Reissner's mixed variational principle. Meccanica 50:2621–2648

Timoshenko SP, Woinowsky-Krieger S (1959) Theory of Plates and Shells. McGraw-Hill, 2 edition

Toledano A, Murakami H (1987) A composite plate theory for arbitrary laminate configurations. J Appl Mech 54:181–189

Touratier M (1991) An efficient standard plate theory. Int J Eng Sci 29:901–916

Vidal P, Polit O (2011) A sine finite element using a zig-zag function for the analysis of laminated composite beams. Compos B 42:1671–1682

Wenzel C, Vidal P, D'Ottavio M, Polit O (2014) Coupling of heterogeneous kinematics and finite element approximations applied to composite beam structures. Compos Struct 116:177–192

Zienkiewicz OC, Taylor RL (2000) The Finite Element Method, volume 2: Solid Mechanics. Butterworth-Heinemann, 5 edition